IUST
Iran University of Science and Technology

Iranian Journal of Electrical and Electronic Engineering

Journal Homepage: ijeee.iust.ac.ir

Analysis of A Novel Quasi-Reflectionless Microstrip Bandpass Filter Using A New Simple Approach

Kaveh Askari*and Soolmaz Abbasalizadeh * (C.A.)

Abstract: This paper proposes a new one-cell single-port microstrip bandpass filter (BPF) named the main cell, which consists of a band-pass section connected with one band-stop section at the input port. Considering the main cell, this paper provides a new two-cell two-port BPF with quasi-reflectionless behavior at its input and output ports. This two-cell two-port BPF is constructed with three sections of a series bandpass filter at the center and two shunt-connected bandstop filters at the input and output ports. Moreover, this paper analyzes the BPF's S-parameters and, to the best of the authors' knowledge, derives its formulas in a closed form, for the first time. Furthermore, to the best of the authors' knowledge, this paper presents a novel approach for determining the filter's cut-off frequency by utilizing the derived S-parameters. This paper compares the calculated results with the simulated to evaluate the analysis. In addition, this paper proposes a three-cell two-port BPF to increase the out-of-band attenuation loss. Finally, this paper manufactures the two-cell and three-cell BPFs on an FR-4 substrate to evaluate the efficiency of the presented concepts. The comparisons between the electromagnetic simulation and the measurement results have good agreements with each other. The measurement results of the three-cell two-port BPF show a center frequency of 2.6 GHz, a bandwidth of 0.27 GHz, and a minimum in-band insertion loss of -3 dB. Also, the fabricated filter has an in-band return loss lower than -8 dB over the entire bandwidth and a stopband attenuation level better than 50 dB.

Keywords: Bandpass filter, Bandstop filter, Cut-off frequency Analysis, Microstrip filter, Reflectionless bandpass filter.

1 Introduction

NOWADAYS, high-frequency applications like the fifth generation (5G) communication systems have gained much attention due to their capability to transfer high data rate, providing the requirement of Gbps communications to multiple users [1]-[3], ultra-low latency communications [4], and convenient wireless access [5].

One of the high-frequency transceivers' main blocks is a bandpass filter (BPF) used to block interference, filter unwanted frequencies, and suppress noise signals [6]-[7]. Since the frequency and quality factor of the on-chip lumped elements limit the operational frequency and performance of the filter, the design of high-performance and high-selectivity microstrip filters is an attractive option for designers to use in these applications [8].

Reference [2] presents a tri-band BPF with tunable operation frequency using a multi-stub loaded resonator with eight resonance modes to cover the 5G WiFi bands. Reference [5] presents a compact BPF that uses two resonators to satisfy the quad-band operations of the filter suitable for multiple high-frequency applications. A tunable bandpass microstrip filter for 5G wireless communications is provided by [6] that uses three open-loop ring resonators ended with an impedance of 50 Ω at input/output ports. Reference [9] proposes, models, and designs an ultra-thin lowpass and bandpass filter on a glass substrate utilizing a Large-area panel-compatible semi-additive patterning (SAP) process for the mm-wave

Iranian Journal of Electrical & Electronic Engineering, 2026.
Paper first received 14 Jul 2025 and accepted 04 Jan 2026.
* The authors are with the Department of Electrical and Biomedical Engineering, Mazandaran University of Science and Technology, Babol, Iran.
E-mails:
kave.askari@gmail.com,s.abasalizade@ustmb.ac.ir.
Corresponding Author: Soolmaz Abbasalizadeh.

applications. However, none of the discussed references analyzed the filter and none of them derived its S-parameters as the essential parameters to understand the design procedure of the filter. Thus, using these references, the designers should use many lengthy simulations to reach an optimum filter structure. Also, the complicated filters' topologies proposed by these references make the fabrication process intricate and expensive. Moreover, these references did not consider the filter's reflectionless property.

The reflectionless RF devices improve the linearity and dynamic range of the RF front-end. Thus, the return loss is a fundamental parameter in the filter design. Some references provide reflectionless filters to prevent unwanted signals from entering the desired bands [10]-[20]. As some examples, references [10] and [12] present the adjustable multiband reflectionless BPFs using the input reflectionless topology and a new class of reflectionless filters, respectively. However, using a large number of lumped elements in the filter topology of [12] limits the operation frequency of the filter and complicates the filter structure. A class of BPFs with quasi-reflectionless behavior on both input and output ports is proposed by [13]. The filter's design procedure and description of its S-parameters are also provided in this reference. However, this reference does not derive the final closed-form formulas of the S-parameters due to their complicated procedure analysis and does not analyze the filter's cut-off frequency. Based on our knowledge, most references on microstrip filters do not employ analytical approaches for filter design. Only some of the limited references employed analytical approaches; however, due to the complexity and size of the presented formulas, it would be challenging for designers to use the proposed formula for filter design.

We propose a BPF with a simpler structure than [13]. We analyze it and derive the closed-form formulas for its S-parameters. We also analyze the cut-off frequency of the filter and obtain the closed-form formula for it. To the best of our knowledge, this approach for deriving the filter's cut-off frequency is presented by this paper for the first time. Moreover, we cascade the proposed BPF to achieve a higher stopband attenuation level. For this purpose, we present a main cell of the filter and use it to construct the reflectionless two-cell two-port BPF. First, we analyze one-cell single-port BPF and use the results to extract the values of each transmission line section in the filter's structure. We also describe the filter's design procedure. Then, we analyze the reflectionless two-cell two-port BPF and derive its S-parameters. Using these closed-form formulas, the designer can design the BPF for any application without using many lengthy simulations.

Contrary to previously reported reflectionless BPF that uses a complicated coupling topology analysis method, we present a simple analysis using [13] and obtain the closed-form formula of the input admittance of the filter. Thus, the designers can easily extract each section's transmission line's characteristic impedance. The analysis proposed in this paper can be a simple design procedure for designers. Finally, using the new simple approach and considering the extracted S-parameters, we derive the BPF's cut-off frequency and attenuation at a particular frequency.

We organize the rest of the paper as follows. Section 2 proposes the main cell of the filter. This section also describes the design procedure. Section 3 presents a reflectionless two-cell two-port BPF, analyzes it, and derives BPF's S-parameters, the cut-off frequency, and the attenuation formulas. The comparison between the simulation and calculation results is also provided in this section to evaluate the presented analysis. This section also proposes the three-cell BPF with the higher out-of-band attenuation. Section 4 provides the electromagnetic simulation and the measurement results to verify the efficiency of the proposed BPFs. Finally, section 5 presents the conclusion.

2 The Main Cell

Fig. 1 shows the main cell of the reflectionless BPF circuit in which θ is the electrical length of the transmission line and $\theta_1 = 2\theta_2$. According to this figure, the cell comprises a high-impedance transmission line (a bandpass section) connected in parallel with a bandstop section. Therefore, we can write $Z_{in} = Z_{BPF\text{-}in} \parallel Z_{BSF\text{-}in}$ or $Y_{in} = Y_{BPF\text{-}in} + Y_{BSF\text{-}in}$, where Z_{in}, $Z_{BPF\text{-}in}$, and $Z_{BSF\text{-}in}$ are the input impedance of the reflectionless BPF's main cell, the input impedance of the bandpass filter section, and the input impedance of the bandstop filter section, respectively. Also, Y_{in}, $Y_{BPF\text{-}in}$, and $Y_{BSF\text{-}in}$ are the input admittance of the reflectionless BPF's main cell, the input admittance of the bandpass filter section, and the input admittance of the bandstop filter section, respectively.

Considering Fig. 1, the circuit input impedance should equal $Z_0 = 50\ \Omega$ over the entire passband to satisfy the BPF reflectionless property. Due to the shunt-connected topology of the bandpass and bandstop filter sections, it is simpler to see the input admittance rather than the impedance to understand this situation. Referring to Fig. 1, we can write the input admittance of the bandpass and bandstop filter section as

$$\begin{aligned} Y_{BPF-in} &= \frac{1}{Z_1}\frac{Z_1 + jZ_0\tan(\theta_1)}{Z_0 + jZ_1\tan(\theta_1)} \\ &= Y_0\left(\frac{1+\tan^2(\theta_1)}{\left(1+Z_{1,0}^2\tan^2(\theta_1)\right)} + j\,\frac{\tan(\theta_1)\left(1-Z_{1,0}^2\right)}{Z_1\left(1+Z_{1,0}^2\tan^2(\theta_1)\right)}\right) \end{aligned} \quad (1)$$

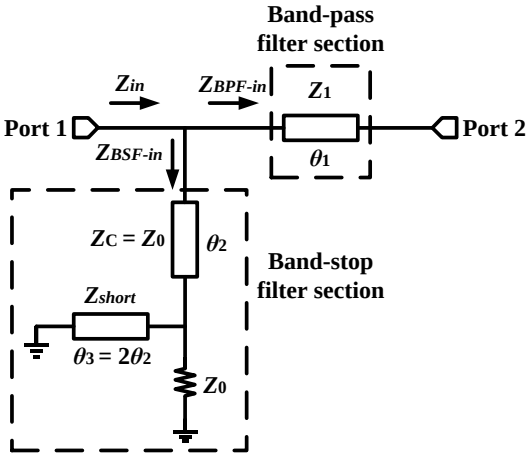

Fig. 1. The main cell.

$$Y_{BSF-in} = \frac{1}{Z_0}\frac{Z_0 + j\left(\left(jZ_0\tan(\theta_3)\right)\|\,Z_0\right)\tan(\theta_2)}{\left(\left(jZ_0\tan(\theta_3)\right)\|\,Z_0\right)+jZ_0\tan(\theta_2)}$$
$$= Y_0\left(\frac{4Z_{sh,0}^2\left(1+\tan^2(\theta_2)\right)-j\dfrac{\left(1-\tan^2(\theta_2)\right)\left(1+2Z_{sh,0}\right)}{\tan(\theta_2)}}{\left(4Z_{sh,0}^2\tan^2(\theta_2)+\left(2Z_{sh,0}+1-\tan^2(\theta_2)\right)^2\right)}\right) \quad (2)$$

In the above equation, Z_0 = 50 Ω (the port impedance), Y_0 = 1/50 (1/Ω) (the port admittance), $Z_{1,0} = Z_1/Z_0$, and $Z_{sh,0} = Z_{short}/Z_0$.

To satisfy the reflectionless property of the filter, $Y_{in} = Y_{BPF-in} + Y_{BSF-in}$ at $\theta_1 = 2\theta_2 = 90^\circ$, $\theta_1 = 2\theta_2 = 180^\circ$, and $\theta_1 = 2\theta_2 = 270^\circ$ should be real and equal to 1/50 (1/Ω). Considering Eq. (1) and Eq. (2), we achieve $Y_{BPF-in} = Y_0$ and $Y_{BSF-in} = 0$ at $\theta_1 = 2\theta_2 = 180^\circ$ which shows that the proposed main cell has a good matching at the center frequency.

Substituting $\theta_1 = 2\theta_2 = 90^\circ$ or $\theta_1 = 2\theta_2 = 270^\circ$ in Eq. (1) and Eq. (2), we obtain $Y_{BPF-in} = Z_0/Z_1^2$ and $Y_{BSF-in} = Y_0$. To achieve $Y_{in} = Y_0$ in $\theta_1 = 2\theta_2 = 90^\circ$ or $\theta_1 = 2\theta_2 = 270^\circ$, Y_{BPF-in} should be zero in these frequencies. Thus, Z_1 should be the possible maximum value according to the fabrication process to satisfy this condition. Considering the FR-4 substrate as the design process, we consider Z_1 = 150 Ω as the possible maximum value.

To extract the best value for Z_{short} that results in the lower S_{11}, we derive the S_{11} parameter of the main cell using Eq. (1) and Eq. (2), plot its magnitude for different Z_{short} using MatLab software, and choose its appropriate value. Using the conventional definition of S_{11} (the return loss), we can write

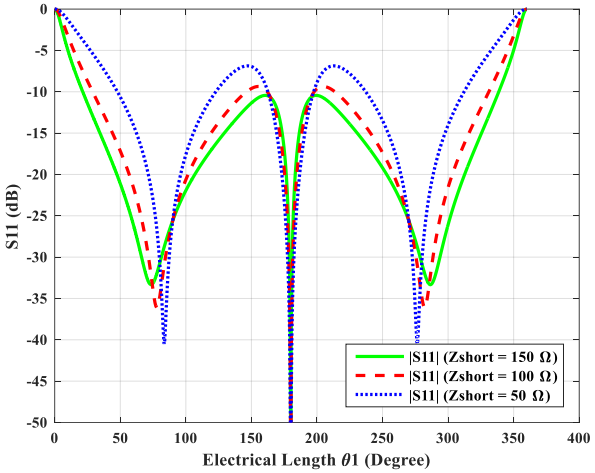

Fig. 2. S_{11} of the main cell for different Z_{short}.

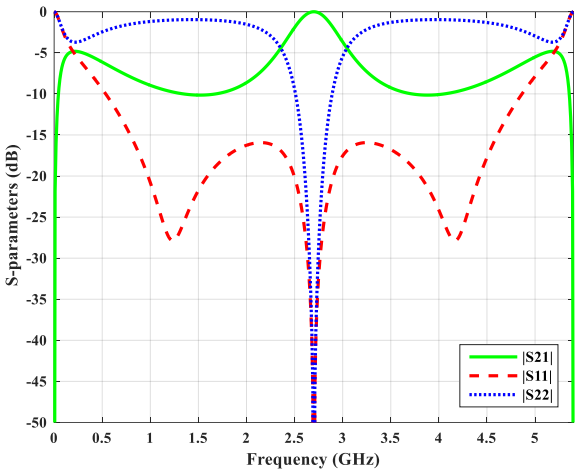

Fig. 3. The simulated S-parameters of the main cell.

$$S_{11} = \frac{Z_{in} - Z_0}{Z_{in} + Z_0} = \frac{1 - \dfrac{\left(Y_{BPF-in} + Y_{BSF-in}\right)}{Y_0}}{1 + \dfrac{\left(Y_{BPF-in} + Y_{BSF-in}\right)}{Y_0}} \quad (3)$$

The magnitude of Eq. (3) for different Z_{short} is plotted in Fig. 2. Based on Fig. 2, the maximum value of Z_{short} leads to less S_{11}. Thus, the impedance of Z_{short} must have its maximum value according to the fabrication process.

Fig. 3 demonstrates the simulated S-parameters of the main cell with ideal transmission lines, characteristic impedances of Z_0 = 50 Ω and $Z_1 = Z_{short}$ = 150 Ω, and using Advanced Design Software (ADS). As can be seen from this figure, the out-of-band reflection of $|S_{22}|$ is larger than the out-of-band value of $|S_{11}|$. Thus, the reflectionless property of the main cell is only achieved at one port (the input port). To obtain the reflectionless

property at both input and output ports, we will propose a reflectionless two-cell two-port BPF in section 3.

3 A Reflectionless Two-Cell Two-Port BPF

Fig. 4 shows the reflectionless two-cell two-port BPF. Compared with the main cell shown in Fig. 1, we have added another bandstop section at the output port of the main cell to achieve the reflectionless property at both input and output ports. Since the circuit in Fig. 4 is symmetric, we use the even and odd modes analysis method to derive the S-parameters of the two-cell two-port reflectionless BPF in the following. Also, using the extracted S-parameters, we will obtain the parameters needed to design the filter.

3.1 S-parameters analysis

Fig. 5(a) and Fig. 5(b) demonstrate the even and odd modes equivalent circuits of two-cell two-port BPF, respectively. For the even mode, the symmetry plane is the perfect magnetic wall while for the odd mode, the central symmetry plane is the ideal electric wall [13].

The Y-matrix of the two-network circuit in Fig. 4 is

$$[Y] = \begin{bmatrix} \frac{Y_{even}+Y_{odd}}{2} & \frac{Y_{even}-Y_{odd}}{2} \\ \frac{Y_{even}-Y_{odd}}{2} & \frac{Y_{even}+Y_{odd}}{2} \end{bmatrix} \quad (4)$$

In the above equation, $Y_{even} = Y_{BPF\text{-}even} + Y_{BSF\text{-}even}$ and $Y_{odd} = Y_{BPF\text{-}odd} + Y_{BSF\text{-}odd}$ are the input admittance of the filter in the even and odd modes, respectively.

Referring to Fig. 5(a) and Fig. 5(b), we can derive $Y_{BPF\text{-}even} = 1/(-jZ_1\cot(\theta_1/2))$ and $Y_{BPF\text{-}odd} = -j/(Z_1\tan(\theta_1/2))$. Also, we can write $Y_{BSF\text{-}even} = Y_{BSF\text{-}odd}$ as

$$Y_{BSF-even} = Y_{BSF-odd} = \frac{Z_C + jZ_L\tan(\theta_2)}{Z_C(Z_L + jZ_C\tan(\theta_2))} \quad (5)$$

where $Z_C = Z_0$ and Z_L is

$$Z_L(\theta_3 = 2\theta_2) = \frac{Z_{short}Z_0\tan(2\theta_2)}{Z_{short}\tan(2\theta_2) - jZ_0} \quad (6)$$

Considering $\tan(2\theta_2) = 2\tan(\theta_2)/(1-\tan^2(\theta_2))$, we rewrite Z_L as

$$Z_L(\theta_2) = \frac{2Z_{short}Z_0}{2Z_{short} - jZ_0\cot(\theta_2) + jZ_0\tan(\theta_2)} \quad (7)$$

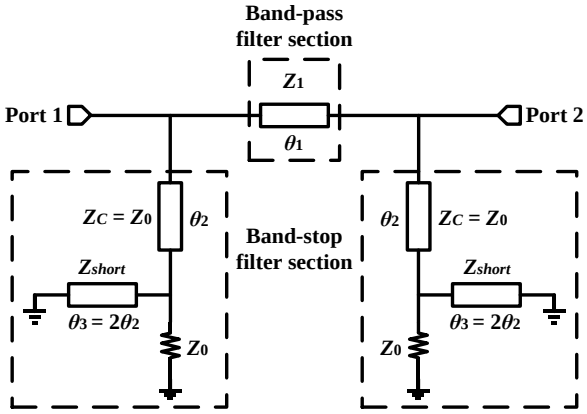

Fig. 4. A reflectionless two-cell two-port BPF.

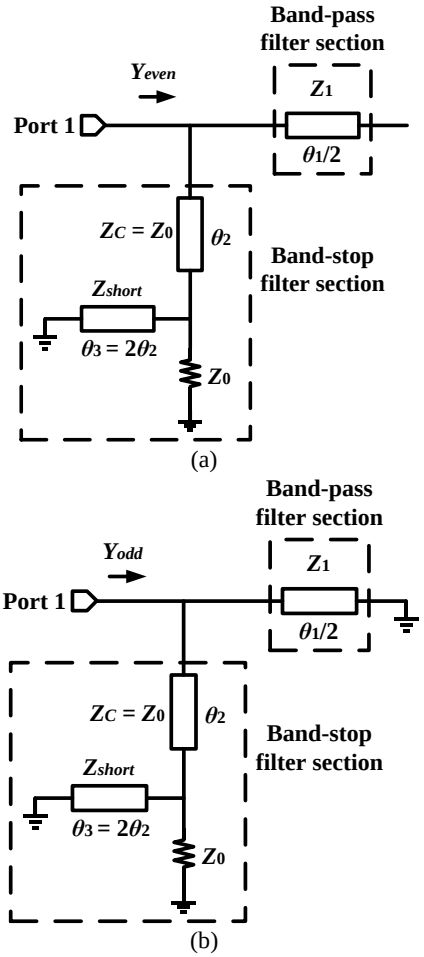

Fig. 5. The reflectionless two-cell two-port BPF's equivalent circuits, (a) Even-mode, (b) Odd-mode.

Substituting Eq. (7) in Eq. (5) and defining $A = \tan(\theta_2)$, $B = 1 + \tan^2(\theta_2)$, and $C = 1 - \tan^2(\theta_2)$, we achieve

$$Y_{BSF-even} = Y_{BSF-odd} = \frac{1}{Z_0} \frac{\frac{4Z_{sh,0}^2 AB}{C^2} - j(1+2Z_{sh,0})}{\left((2Z_{sh,0}A)^2 + (2Z_{sh,0}+C)^2\right)\frac{A}{C^2}} \quad (8)$$

According to [13], we can write the S-parameters of the reflectionless two-cell two-port BPF as

$$S_{11} = \frac{Y_0^2 - Y_{even}Y_{odd}}{(Y_0+Y_{odd})(Y_0+Y_{even})} \quad (9)$$

$$S_{21} = \frac{Y_0(Y_{even}-Y_{odd})}{(Y_0+Y_{odd})(Y_0+Y_{even})} \quad (10)$$

In the above equations, $Y_{even} = (jA/Z_1) + Y_{BSF\text{-}even}$ and $Y_{odd} = (-j/(AZ_1)) + Y_{BSF\text{-}odd}$.

Substituting Y_{even} and Y_{odd} in Eq. (9) and Eq. (10) and using Eq. (8), we obtain the S-parameters of the reflectionless two-cell two-port BPF as

$$S_{11} = \frac{1 - E^2 - \frac{1}{Z_{1,0}^2} + j\frac{EC}{Z_{1,0}A}}{(1+E)^2 + \frac{1}{Z_{1,0}^2} - j\frac{(1+E)C}{Z_{1,0}A}} \quad (11)$$

$$S_{21} = \frac{Y_0 Z_1}{\left(\frac{Z_{1,0}CF}{D}\right) + j\left(\frac{Z_{1,0}^2 ABF^2}{D^2} + \frac{A}{B}\right)} \quad (12)$$

where

$$E = \frac{4Z_{sh,0}^2 AB - jC^2(1+2Z_{sh,0})}{AD} \quad (13)$$

$$D = (2Z_{sh,0}A)^2 + (2Z_{sh,0}+C)^2 \quad (14)$$

$$F = 8Z_{sh,0}^2 + \frac{C(C+4Z_{sh,0})}{B} - j\frac{(1+2Z_{sh,0})C^2}{AB} \quad (15)$$

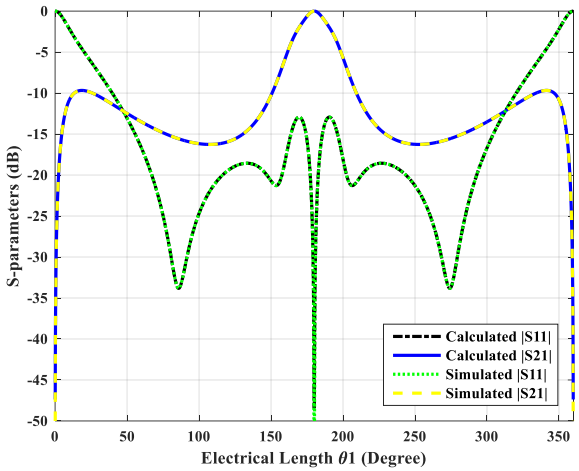

Fig. 6. Comparison between the calculated and the simulated S-parameters of the reflectionless two-cell two-port BPF versus θ_1.

To evaluate the validity of the S_{11} and S_{21} analytical formulas (Eq. (11) and Eq. (12)), we have compared the calculated results with the simulated results in Fig. 6. In this figure, S-parameters are shown versus the electrical length of θ_1. In the comparison, we have used $Z_1 = Z_{short} = 150\ \Omega$ and $Z_0 = Z_C = 50\ \Omega$. To simulate the BPF with the ADS software, we have constructed the filter with the ideal transmission lines based on Fig. 4. As can be seen from the comparison, the calculated and the simulated results agree well with each other.

3.2 The two-cell two-port BPF's cut-off frequency analysis

Since the cut-off frequency and the attenuation of the BPF are important parameters for filter designing, we consider Eq. (12), extract $|S_{21}|$, and use the final formula to obtain the mentioned parameters. We use the new simple method to derive the proposed BPF's cut-off frequency formulas.

$|S_{21}|$ is

$$|S_{21}| = \frac{1}{\sqrt{\left(\frac{A}{B}Z_1Y_0\left((1+E_1)^2 - E_2^2\right) + \frac{A}{BY_0Z_1} + \frac{C}{B}E_2\right)^2 + \left(\left(2\frac{A}{B}Z_1Y_0E_2 - \frac{C}{B}\right)(1+E_1)\right)^2}} \quad (16)$$

where $E_1 = 4Z_{sh,0}^2 B/D$ and $E_2 = -C^2(1 + 2\,Z_{sh,0})/(AD)$.

To evaluate the proposed BPF's insertion loss, we substitute the center frequency ($\theta_2 = 90^\circ$) in Eq. (16) and reach $|S_{21}| = 0$. This confirms the proposed BPF's efficiency in passing the desired signals.

To derive the proposed BPF's cut-off frequency, we should refer to Eq. (16) and use $|S_{21}| = 1/\sqrt{2}$. But $|S_{21}|$ in Eq. (16) is a complicated formula which makes the cut-off frequency analysis hard. To overcome this complexity, we have considered an optimistic assumption. We assume the BPF in Fig. 4 is a sharp-rejection filter. Using this, we can approximate Eq. (16) to a simple formula. Since we proposed the BPF for high-frequency applications, where the BPF center frequency is much higher than the bandwidth, this assumption is appropriate. It should be noted that based on our survey, this cut-off frequency analysis method for microstrip filters is proposed for the first time in this paper.

Based on the above discussion, we can rewrite $A = \tan(\theta_2) = \tan((\pi/2) + \Delta\theta) = -\cot(\Delta\theta) \approx -1/\Delta\theta$, in which $\Delta\theta$ is the cut-off frequency in radians. With the same procedure and assuming a small value for $\Delta\theta$, we can approximate $B \approx 1/(\Delta\theta)^2$ and $C \approx -1/(\Delta\theta)^2$. Substituting the approximated A, B, and C in D, E_1, and E_2 and ignoring the small terms, we obtain

$$D \approx \frac{4Z_{sh,0}(Z_{sh,0}-1)}{(\Delta\theta)^2} + \frac{1}{(\Delta\theta)^4} \tag{17}$$

$$E_1 \approx \frac{4Z_{sh,0}^2}{4Z_{sh,0}(Z_{sh,0}-1) + \dfrac{1}{(\Delta\theta)^2}} \tag{18}$$

$$E_2 \approx (\Delta\theta)\left(1+2Z_{sh,0}\right) \tag{19}$$

Substituting the approximated parameters of A, B, C, D, E_1, and E_2 in Eq. (16) and ignoring the small terms with higher orders, we derive the approximated $|S_{21}|$ as

$$|S_{21}| \approx \frac{\left(4Z_{sh,0}(Z_{sh,0}-1)(\Delta\theta)^2+1\right)^2}{\sqrt{G}} \tag{20}$$

In the above equation, G is

$$\begin{aligned} G &= 32K_1K_3(\Delta\theta)^8 + \left(K_1^2 + 32K_2K_3\right)(\Delta\theta)^6 \\ &+2\left(K_1K_2 + 8K_4^2\right)(\Delta\theta)^4 + \left(K_2^2 + 8K_4\right)(\Delta\theta)^2 + 1 \end{aligned} \tag{21}$$

where

$$K_1 = Z_1Y_0\left(12Z_{sh,0}^2 - 12Z_{sh,0} - 1\right) + 8Z_{sh,0}(2Z_{sh,0}^2 - Z_{sh,0} - 1) \tag{22}$$

$$K_2 = Z_1Y_0 + 1 + 2Z_{sh,0} \tag{23}$$

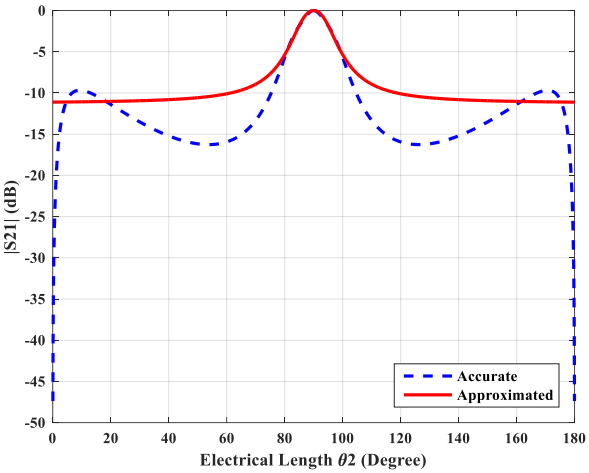

Fig. 7. Comparison between the accurate and approximated $|S_{21}|$.

$$K_3 = Z_{sh,0}^2(Z_{sh,0}-1)^2\left(1+2Z_{sh,0}\right) \tag{24}$$

$$K_4 = Z_{sh,0}(Z_{sh,0}-1) \tag{25}$$

To evaluate the approximated $|S_{21}|$, we have plotted Eq. (16) and Eq. (20) in Fig. 7 by considering $Z_1 = Z_{short} = 150\ \Omega$ and $Z_0 = Z_C = 50\ \Omega$. According to this figure, Eq. (20) is a good approximation of Eq. (16) in the bandwidth range of the proposed two-cell BPF.

To derive the cut-off frequency of the proposed BPF, we use Eq. (20), solve the equation of $|S_{21}| = 1/\sqrt{2}$, and achieve

$$\begin{aligned} &\left(32K_1K_3 - 512K_4^4\right)(\Delta\theta)^8 + \left(K_1^2 + 32K_2K_3 - 512K_4^3\right)(\Delta\theta)^6 \\ &+\left(2K_1K_2 - 176K_4^2\right)(\Delta\theta)^4 + \left(K_2^2 - 24K_4\right)(\Delta\theta)^2 - 1 = 0 \end{aligned} \tag{26}$$

The above equation is an 8th-order equation and can be solved with numerical methods using MatLab software. Since the numerical method does not lead to an accurate closed-form solution for the equation, we have used the fitted curve approximation using the MatLab software to obtain the closed-form solution for the cut-off frequency of the proposed two-cell BPF. The approximated closed-form formula for the cut-off frequency is

$$\Delta\theta \approx \sqrt[4]{\frac{-\left(K_1K_2 - 88K_4^2\right) + \sqrt{\left(K_1K_2 - 88K_4^2\right)^2 + \left(32K_1K_3 - 512K_4^4\right)}}{32K_1K_3 - 512K_4^4}} \tag{27}$$

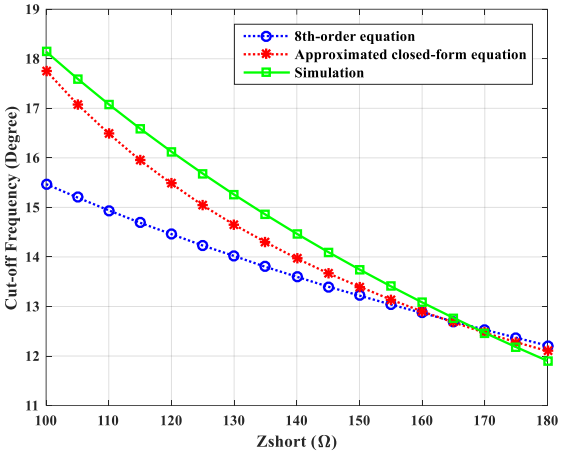

Fig. 8. Comparison between the calculated and simulated results of the cut-off frequency.

To verify the accuracy of the presented cut-off frequency analysis, we have compared the simulated results with the calculated based on Eq. (26) and Eq. (27). In the simulation, we have constructed the BPF with the ideal transmission lines, the characteristic impedance of $Z_1 = 150\ \Omega$, and $Z_0 = Z_C = 50\ \Omega$. Also, we have varied the impedance of the shorted transmission line (Z_{short}) from 100 Ω to 180 Ω. Fig. 8 shows the comparison between the simulated and calculated results. According to this figure, the maximum deviation between the calculated and simulated results is 14.7% and 4.1% based on Eq. (26) and Eq. (27), respectively. These results show the accuracy of the proposed approximated cut-off frequency analysis. It should be noted that Eq. (26) and Eq. (27) lead to approximate results for the filter's cut-off frequency. Based on Fig. 8, the proposed approximated equation is more valid for higher values of Z_{short}, where the cut-off frequency is smaller, due to a sharp-rejection assumption in the analysis. As mentioned earlier, to overcome the cut-off frequency complicated analysis, we had assumed that the filter has a much higher center frequency than its bandwidth. Therefore, the proposed analysis and the derived formulas are more valid for the sharp cut-off frequency and have limitations for use in a wideband microstrip filter.

Considering Eq. (26) and Eq. (27), as well as Fig. 8, designers can determine the Z_{short} value based on their specific bandwidth to design the proposed filter for their respective applications. Additionally, the proposed equations provide designers with valuable insight into designing a new filter with a tunable cut-off frequency.

3.3 The two-cell BPF's out-of-band attenuation analysis

As we know, the out-of-band attenuation of the filter is an important parameter when choosing the type of filter. The frequency at which the out-of-band attenuation is calculated depends on the used application and its required specifications. Here, to get the proper view of the out-of-band attenuation of the proposed BPF, we consider the center frequency of the BPF as $\theta_2 = 90^\circ$ and extract the attenuation of the two-cell BPF at a particular frequency ($\theta_2 = 120^\circ$). To simplify the analysis, we substitute $Z_1 = 150\ \Omega$ in Eq. (16) and derive $|S_{21}|$ at $\theta_2 = 120^\circ$. The result is

$$\left|S_{21}\right|_{\theta_2=120^\circ} = \frac{\left(4Z_{sh,0}^{2} - 2Z_{sh,0} + 1\right)^2}{\sqrt{H}} \tag{28}$$

where

$$H = 7557.333Z_{sh,0}^{8} - 8256Z_{sh,0}^{7} + 7528Z_{sh,0}^{6} - 3650.6667Z_{sh,0}^{5} + 1637Z_{sh,0}^{4} - 434Z_{sh,0}^{3} + 123.833Z_{sh,0}^{2} - 15.5Z_{sh,0} + 2.6875 \tag{29}$$

Considering the above equation, since $Z_{sh,0} = Z_{short}/Z_0 > 1$, we can ignore the small terms with small coefficients and small orders in H. We can approximate $H \approx 7557.33\ Z^5_{sh,0}\ (Z^3_{sh,0} - 1.092\ Z^2_{sh,0} + 0.996\ Z_{sh,0} - 0.483)$. Also, we can round the numbers in H and rewrite $H \approx 7557.33\ Z^5_{sh,0}\ (Z^3_{sh,0} - Z^2_{sh,0} + Z_{sh,0})$. Using this, we obtain the out-of-band attenuation of the proposed two-cell BPF as

$$\left|S_{21}\right|_{\theta_2=120^\circ} \approx \frac{\left(4Z_{sh,0}^{2} - 2Z_{sh,0} + 1\right)^2}{87Z_{sh,0}^{3}\sqrt{Z_{sh,0}^{2} - Z_{sh,0} + 1}} \tag{30}$$

To evaluate the accuracy of the obtained attenuation formula, we have simulated the BPF with different Z_{short}, $Z_1 = 150\ \Omega$, and $Z_0 = Z_C = 50\ \Omega$. We have calculated the out-of-band attenuation based on Eq. (28) and Eq. (30) and compared the results with the simulation in Fig. 9. Based on this figure, there is a good agreement between the simulated and the calculated results. The maximum deviation between the simulated and calculated results is 1.28% for the approximated attenuation equation, which shows the accuracy of Eq. (30).

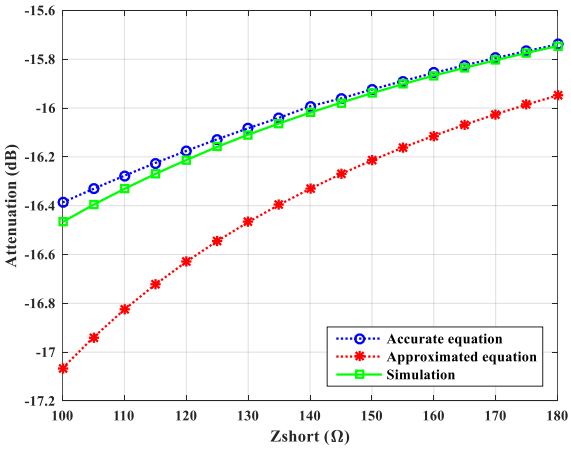

Fig. 9. Comparison between the calculated and simulated results of the out-of-band attenuation at $\theta_2 = 120^\circ$.

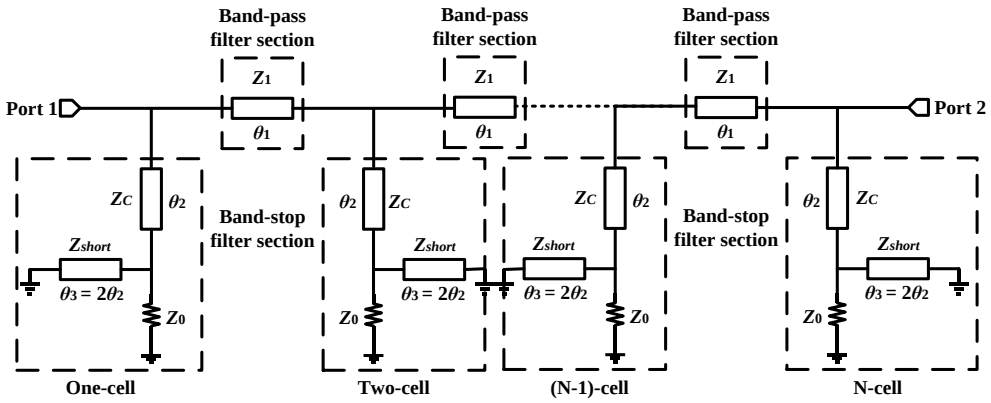

Fig. 10. A reflectionless N-cell two-port BPF.

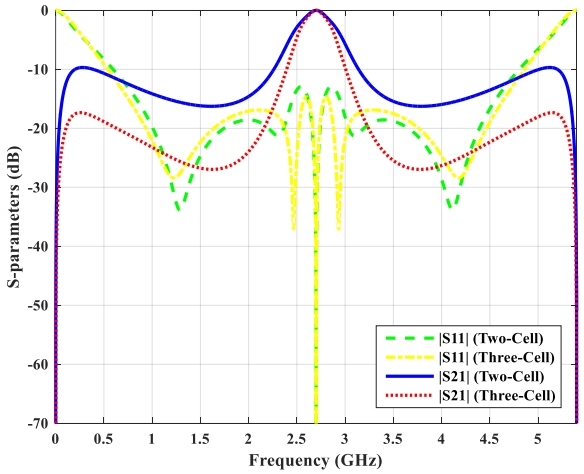

Fig. 11. The comparison between the S-parameters of the reflectionless two-cell and three cell BPFs.

Table 1 FR-4 Substrate Specifications.

Relative Dielectric Permittivity (εr)	Dielectric Thickness (H)	Metal Thickness (t)	Dielectric Loss Tangent ($\tan\delta$)
4.5	1.57 mm	0.035 mm	0.019

3.4 Higher order BPF

Considering Fig. 4, we can cascade the reflectionless two-cell two-port BPF to increase the filter's order and the out-of-band attenuation. Fig. 10 shows the reflectionless N-cell two-port BPF containing N bandstop sections. In addition, Fig. 11 demonstrates the simulated S-parameters of the two-cell and three-cell BPFs for comparison. As can be seen from this figure, cascading more cells leads to a sharper frequency response curve and more out-of-band attenuation. Based on Fig. 11, the three-cell BPF has a 322 MHz bandwidth and better out-of-band attenuation than the two-cell two-port BPF.

4 Measurment Results

In this section, we first provide the electromagnetic (EM) simulation using Agilent High-Frequency Structure Software (HFSS) to evaluate the validity and accuracy of the proposed reflectionless BPF after fabrication. We have used the FR-4 substrate with the specifications listed in Table 1, where $Z_{short} = Z_1 = 150\ \Omega$ and $Z_0 = Z_C = 50\ \Omega$. Using a FR-4 substrate with a 1.57 mm dielectric thickness for a given transmission line width and specified dielectric loss tangent, helps us achieve a 150 Ω characteristic impedance for our transmission lines. It should be noted that although increasing the substrate dielectric thickness leads to lower conductor loss and higher characteristic impedance for a given line width, it can hurt stop-band rejection.

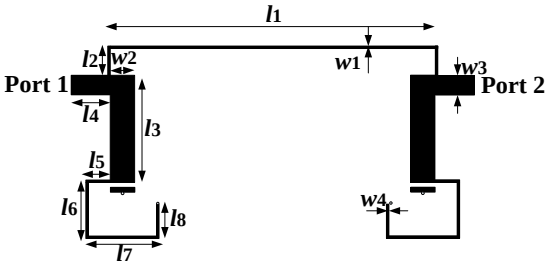

(a)

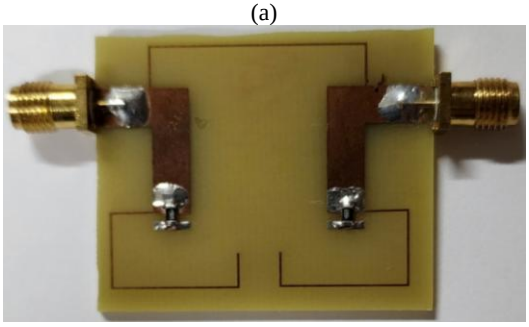

(b)

Fig. 12. The two-cell two-port reflectionless BPF. (a) physical dimensions in mm: $l_1 = 25.4$, $l_2 = 5$, $l_3 = 15$, $l_4 = 7.3$, $l_5 = 5.3$, $l_6 = 9$, $l_7 = 15$, $l_8 = 4$, $w_1 = 0.3$, $w_2 = 4.5$, $w_3 = 4.5$, $w_4 = 0.3$, (b) photograph.

Secondly, we have implemented the two-cell and three-cell two-port BPFs on the FR-4 substrate. We have used the Agilent N5230A network analyzer to measure the S-parameters of the fabricated BPFs. Finally, we have compared the simulated and measured results to evaluate the efficiency of the proposed BPFs.

Fig. 12 demonstrates the physical dimensions and photograph of the two-cell two-port BPF. The physical dimensions and photograph of the three-cell two-port BPF are also shown in Fig. 13. Considering Fig. 12 and Fig. 13, the overall dimensions of the two-cell and three-cell two-port BPFs are 40 × 33 mm^2 and 76 × 33 mm^2, respectively.

The simulated and the measured S-parameters of the two-cell and three-cell two-port BPFs are compared in Fig. 14 and Fig. 15, respectively. As can be seen, there is a deviation between the simulated and measured center frequencies and the return loss. This is caused by the fabrication tolerance. Based on Fig. 14, the fabricated two-cell BPF has a center frequency of 2.6 GHz, a 3-dB absolute bandwidth of 0.37 GHz (14% of fractional bandwidth), a minimum insertion loss of -2 dB, a return loss smaller than -6 dB in the range of the bandwidth, and the stopband attenuation level better than 25 dB.

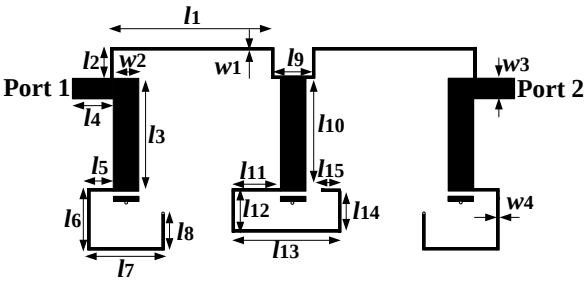

(a)

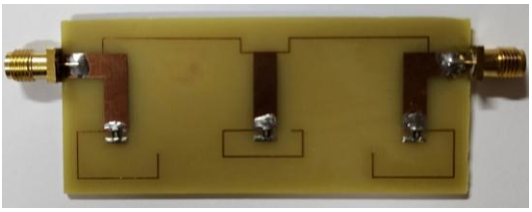

(b)

Fig. 13. The three-cell two-port reflectionless BPF. (a) physical dimensions in mm: l_1 = 25.9, l_2 = 3, l_3 = 15, l_4 = 7.3, l_5 = 5.3, l_6 = 9, l_7 = 15, l_8 = 4.5, l_9 = 9, l_{10} = 15, l_{11} = 6, l_{12} = 5, l_{13} = 15, l_{14} = 5, l_{15} = 2, w_1 = 0.3, w_2 = 4.5, w_3 = 4.5, w_4 = 0.3, (b) photograph.

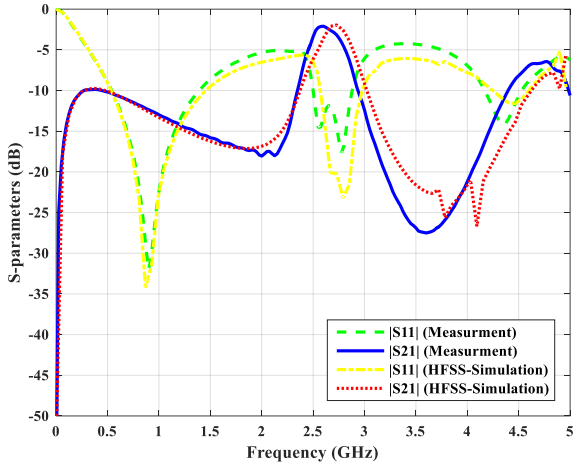

Fig. 14. The comparison between the simulated and measured S-parameters of the two-cell two-port BPF.

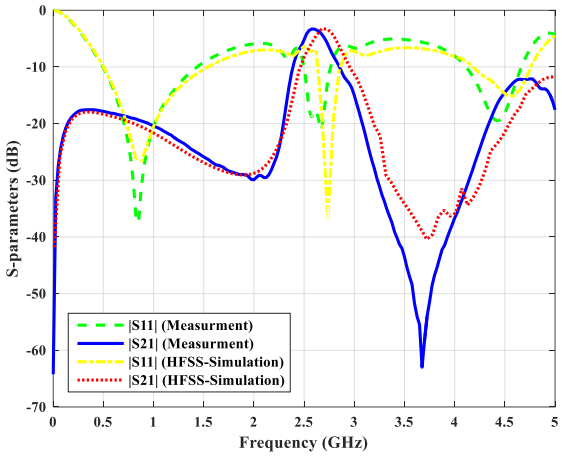

Fig. 15. The comparison between the simulated and measured S-parameters of the three-cell two-port BPF.

Also, the fabricated three-cell BPF has a center frequency of 2.6 GHz, a 3-dB absolute bandwidth of 0.27 GHz (10% of fractional bandwidth), a minimum insertion loss of -3 dB, a return loss smaller than -8 dB in the range of bandwidth, and the stopband attenuation level better than 50 dB. Considering this attenuation level, the high selectivity of the three-cell two-port BPF is apparent. It should be noted that using other substrates, such as Rogers, may lead to achieving better performance for the designed filters. FR-4 substrate has higher dielectric loss, lower characteristic impedance, and slower signal propagation compared to Rogers. But due to FR-4 substrate's low cost, easy fabrication, and smaller size, we have chosen it for the filter implementation.

Table 2 Comparisons with Some Previous Works.

	This work (Two-cell)	This work (Three-cell)	[13] 2020	[21]-I 2024	[21]-II 2024	[22] 2025
Substrate	FR-4	FR-4	RO5880	F4BM	F4BM	F4B
Center Frequency (GHz)	2.6	2.6	1.97	3.09	3.25	2
3-dB Absolute Bandwidth (GHz)	0.37	0.27	0.46	0.76	1.858	1.6
Insertion Loss at the Center Frequency (dB)	2	3	0.71	1.26	1.42	3.4
Return Loss in the Range of Bandwidth (dB)	6	8	10	13.1	10	10
Stopband Attenuation Level (dB)	25	50	25	25	40	30
Overall Dimensions (mm^2)	40 × 33	76 × 33	Not reported	Not reported	Not reported	72 × 52.5

5 Conclusion

In this paper, we have proposed a quasi-reflectionless microstrip bandpass filter (BPF) suitable for high-frequency applications. The proposed two-cell two-port BPF is constructed with three sections consisting of a bandpass filter at the center and two bandstop filters connected in parallel with the bandpass filter at the input and output ports. Moreover, we have analyzed the two-cell BPF and derived its S-parameters. We have proposed a new method to extract the cut-off frequency of the BPF using the approximated S-parameters. Also, we have obtained the attenuation of the BPF at a particular frequency. Considering the derived equations, designers can design the proposed two-cell BPF for various applications that have specific cut-off frequencies and attenuation levels without many lengthy simulations. We have provided a comparison between the simulated and calculated results to verify the presented analysis. The comparison shows a good agreement between the simulation and calculation. We also have proposed the three-cell two-port BPF to improve the out-of-band attenuation. Using the electromagnetic simulation with the Agilent High-Frequency Structure Software (HFSS), we have guaranteed the validity of the proposed BPFs after fabrication. Moreover, we have implemented the two-cell and three-cell two-port BPFs on the FR-4 substrate, compared the HFSS simulated and measured results, and shown agreements between the results of the HFSS simulation and the measurement.

Conflict of Interest

The authors declare no conflict of interest.

Author Contributions

Kave Askari: Design, simulate and implement of a new filter. Circuit analysis and derive the filter's parameters formulas. Soolmaz Abbasalizadeh: Design and simulate of a new filter. Circuit analysis and derive the filter's parameters formulas. Writing and reviewing the article.

Funding

No funding was received for this work.

Informed Consent Statement

Not applicable.

Declaration of generative AI and AI-assisted technologies

The authors declare that no generative AI or AI-assisted technologies were used in the writing process of this manuscript.

References

[1] Junning Jiang, Jusung Kim, Aydin Ilker Karsilayan, and Jose Silva-Martinez, "A 3–6-GHz highly linear I-channel receiver with over +3.0-dBm in-band P1dB and 200-MHz baseband bandwidth suitable for 5G wireless and cognitive radio applications," *IEEE Trans. Circuits Syst. I, Regular Papers*, Vol. 66, No. 8, pp. 3134 - 3147, Aug. 2019.

[2] Li Gao, Xiu Yin Zhang, and Quan Xue, "Compact tri-band bandpass filter using novel eight-mode resonator for 5G WiFi application," *IEEE Microw. Wireless Compon. Lett.*, Vol. 25, No. 10, pp. 660-662, Oct. 2015.

[3] Li Gao and Gabriel M. Rebeiz, "Wideband bandpass filter for 5G millimeter-wave application in 45-nm CMOS silicon-on-insulator," *IEEE Elec. Devic. Lett.*, Vol. 42, No. 8, pp. 1244-1247, Aug. 2021.

[4] Huanbo Li, Jixin Chen, Debin Hou, Zekun Li, Zuojun Wang, and Wei Hong, "A high-linearity adaptive-bias SiGe power amplifier for 5G communication," *IEEE Trans. Circuits Syst. II, Exp. Briefs*, Vol. 68, No. 8, pp. 2770-2774, Aug. 2021.

[5] Yao Zhang, Li Gao, and Xiu Yin Zhang, "Compact quad-band bandpass filter for DCS/WLAN/WiMAX/5G Wi-Fi application," *IEEE*

Microw. Wireless Compon. Lett., Vol. 25, No. 10, pp. 645-647, Oct. 2015.

[6] Yasir I. A. Al-Yasir, Naser Ojaroudi Parchin, Ali Alabdallah, Ahmed M. Abdulkhaleq, Raed A. Abd-Alhameed, and James M. Noras, "Design of bandpass tunable filter for green flexible RF for 5G," in IEEE 2nd 5G World Forum (5GWF), Sep. 2019, pp. 194-198.

[7] Cheng-Xiang Wang, Fourat Haider; Xiqi Gao, Xiao-Hu You, Yang Yang and Dongfeng Yuan, "Cellular architecture and key technologies for 5G wireless communication networks," *IEEE Communications Magazine*, Vol. 52, No. 2, pp. 122-130, Feb. 2014.

[8] H. Zhu, X. Zhu, Y. Yang, and Q Xue, "Design of wideband third-order bandpass filters using broadside-coupled resonators in 0.13-μm (Bi)-CMOS technology," *IEEE Trans. Microw. Theory Techn.*, Vol. 66, No. 12, pp. 5593-5604, Dec. 2018.

[9] Muhammad Ali, Fuhan Liu, Atom Watanabe, P. Markondeya Raj, Venkatesh Sundaram, Manos M. Tentzeris, and Rao R. Tummala, "First demonstration of compact, ultra-thin low-pass and bandpass filters for 5G small-cell applications," *IEEE Microw. Wireless Compon. Lett*., Vol. 28, No. 12, pp. 1110-1112, Dec. 2018.

[10] R. Gómez-García, J. Muñoz-Ferreras and D. Psychogiou, "Dual-behavior resonator-based fully reconfigurable input reflectionless bandpass filters," *IEEE Microw. Wireless Compon. Lett*., Vol. 29, No. 1, pp. 35-37, Jan. 2019.

[11] R. Gómez-García, J. Mu-Ferreras, and D. Psychogiou, "Split-Type input reflectionless multiband filters," *IEEE Microw. Wireless Compon. Lett*., Vol. 28, No. 11, pp. 981-983, Nov. 2018.

[12] M. A. Morgan and T. A. Boyd, "Theoretical and experimental study of a new class of reflectionless filter," *IEEE Trans. Microw. Theory Techn*., Vol. 59, No. 5, pp. 1214-1221, May 2011.

[13] Cong Luo, Sai-Wai Wong, Jing-Yu Lin, Yang Yang, Yin Li, Xu-Zhou Yu, Lin-Ping Feng, and Zhi-Hong Tu, Lei Zhu, "Quasi-reflectionless microstrip bandpass filters using bandstop filter for out-of-band improvement," *IEEE Trans. Circuits Syst. II, Exp. Briefs*, Vol. 67, No. 10, pp. 1849-1853, Oct. 2020.

[14] D. Psychogiou and R. Gómez-García, "Reflectionless adaptive RF filters: bandpass, bandstop, and cascade designs," *IEEE Trans. Microw. Theory Techn*., Vol. 65, No. 11, pp. 4593-4605, Nov. 2017.

[15] Roberto Gomez-Garcia, Dimitra Psychogiou, Jose-Maria Munoz-Ferreras and Li Yang, "Avoiding RF isolators: reflectionless microwave bandpass filtering components for advanced rf front ends," *IEEE Microw. Magazine*, Vol. 21, No. 12, pp. 68-86, Dec. 2020.

[16] Mohamed Malki, Li Yang and Roberto Gómez-García, "Input-reflectionless quasi-elliptic-type single- and dual-band bandpass filters based on passive channelized principles," *IEEE Trans. Circuits Syst. I*, Vol. 70, No. 1, pp. 190-202, Jan. 2023.

[17] Feng Wei, Yu-Chen Xue, Xi-Bei Zhao, Wei-Shen Liu, Le Xu and Peng Fei Zhang, "Balanced BPF with dual-port quasi-reflectionless characteristic and selectivity enhancement," *IEEE Trans. Circuits Syst. II, Exp. Briefs*, Vol. 70, No. 3, pp. 994-998, March 2023.

[18] Kai-Da Xu, Sen Lu, Ying-Jiang Guo and Qiang Chen, "Quasi-reflectionless filters using simple coupled line and t-shaped microstrip structures," *IEEE J. of Radio Frequency Identification*, Vol. 6, pp. 54-63, Aug. 2021.

[19] Li Yang, Roberto Gómez-García, Maoyu Fan and Runqi Zhang, "Multilayered input-reflectionless quasi-elliptic-type wideband bandpass filtering devices on diplexer-based structures," *IEEE Trans. Microw. Theory Techn*., Vol. 70, No. 1, pp. 122-138, Jan. 2022.

[20] Siran Zhang, Hongmei Liu, Zhongbao Wang and Shaojun Fang, "Design of wideband quasi-reflectionless filter with high selectivity and flat passband," *IEEE Trans. Circuits Syst. II, Exp. Briefs*, Vol. 70, No. 11, pp. 4038-4042, Nov. 2023.

[21] Feng Wei, Kai-Xuan Wang, Zeng-Hui Shi, Jia-Qi Wang, Le Xu and Qiwei Li, "Design of differential absorptive bpfs with enhanced differential-mode return loss," *IEEE Trans. Circuits Syst. II, Exp. Briefs*, Vol. 71, No. 9, pp. 4161-4165, Sep. 2024.

[22] Jianxing Li, Jitao Chen, Weiyu He, Yi Song, Zhongxian Zheng and Kai-Da Xu, "A wideband continuously-tunable quasi-reflectionless filtering attenuator," *IEEE Microw. Wireless Technol. Lett.*, Vol. 35, No. 9, pp. 1304-1307, Sep. 2025.

Biographies

Kaveh Askari was born in Babolsar, Iran, in 1973. He received a B.Sc. degree in electronics engineering from the Babol Noshirvani University of Technology, Babol, Iran, in 1997, and a M.Sc. degree from the Mazandaran University of Science and Technology, Babol, Iran, in 2023. His research interests are RF and microwave microelectronics, transmission line-based circuits, and microstrip filters.

Soolmaz Abbasalizadeh received a B.Sc. degree in electrical engineering from the Babol Noshirvani University of Technology, Babol, Iran, in 2009, a M.Sc. from the University of Tehran, Tehran, Iran in 2013, and a Ph.D. degree from Babol Noshirvani University of Technology, Babol, Iran, in 2018. Her research interests are analog integrated circuits design, low power low voltage analog circuits, high-frequency oscillators, transmission line-based oscillators, and microstrip filters. She is currently an assistant professor at the Mazandaran University of Science and Technology, Babol, Iran.